Proceedings of the XVIII International Symposium on Dynamic Problems of Mechanics (DINAME 2019),
M.A. Savi, T.G. Ritto and W.M. Bessa (editors), ABCM, Buzios, RJ, Brazil, March 10th to 15th, 2019

Experimental and numerical vibration analyses of tow-steered composite plates

Daniel A. Pereira[1,3], **Thiago A. M. Guimarães**[2], **and Domingos A. Rade**[1]

[1] ITA - Aeronautics Institute of Technology, Division of Mechanical Engineering, São José dos Campos, Brazil

[2] UFU - Federal University of Uberlândia, School of Mechanical Engineering, Uberlândia, Brazil

[3] IPT - Institute for Technological Research, Lightweight Structures Laboratory, São José dos Campos, Brazil

Abstract: New materials have been providing more flexibility in designing of lightweight structures. Among these materials, fiber reinforced composite materials have been attracting a great deal of attention. Hence, a deep understanding not only of static but also of the dynamic characteristics of composite structures is of primary concern. In particular, the understanding of the damping mechanisms is necessary for improved designs, despite the fact that modeling and characterization of dissipation effects are deemed difficult tasks. Previous studies show that carbon-fiber reinforced polymers (CFRP) can be designed in terms of damping characteristics by acting on its physical and geometric features. In recent years, advances in manufacturing processes have made it possible to consider non-conventional designs in order to improve the properties of composite materials. In particular, the development of automatic fiber placement (AFP) allows the realization of variable stiffness composite laminates (VSCL), among which tow-steered composites, in which continuous fibers follow curvilinear paths, are considered very promising. Therefore, the objective of this paper is to present an experimental and numerical assessment of the influence of fiber steering on the modal damping of CFRP plates for different fiber trajectories. The dynamic model is derived by using a semi-analytical approach based on the combination of the Classical Lamination Theory with the Rayleigh-Ritz (Assumed-Modes) approach. The modal damping factors are calculated using the Strain Energy Method, which is based on the ratio between the stored and the dissipated energies, giving the specific damping capacity (SDC) for each vibration mode. The results have shown that, indeed, fiber steering can exert strong influence on the modal damping factors of composite plates, and the numerical prediction of natural frequencies and modal shapes correlate quite well with the experimental counterparts for both the constant-stiffness and tow-steered plates.

Keywords: CFRP, damping, SDC, tow steering, variable stiffness composites, strain energy method

INTRODUCTION

It is broadly known that composite materials, especially fiber-reinforced ones, have enormous potential for applications to lightweight structures. One of the main advantages of these materials is the possibility of being designed to comply with specific performance criteria by changing the relative fiber orientations of the plies. In addition, new advances in Automated Fiber Placement (AFP) technology currently enables the manufacturing of variable stiffness composite laminates (VSCL), which include tow-steered laminates, in which the continuous fibers are deposited following arbitrarily curvilinear paths. These advances open new possibilities in comparison with the traditional constant-stiffness composite laminates (CSCL) (Ribeiro *et al.*, 2014). As compared to traditional composite laminates, VSCL provides the designer with a broader range of options to design composite structures considering multiple design goals. Under these motivations, researchers have been investigating the influence of fiber steering on the dynamic and aeroelastic behaviors of VSCL (Akhavan and Ribeiro, 2011; Guimarães, 2016). Nonetheless, few works conducted experimental validation (Falcó *et al.*, 2017; Rodrigues *et al.*, 2013).

In terms of vibration behavior, damping of composite materials can be several orders of magnitude higher than that of traditional engineering materials, making them appealing for use in components undergoing dynamic loading (Treviso *et al.*, 2015). Various authors have investigated the influence of layup on the damping levels of traditional composite plates (Saravanos and Chamis, 1990; Hwang *et al.*, 1992; Berthelot, 2006; Abbaslou and Maheri, 2016). However, to the authors' best knowledge, studies on the damping characteristics of tow-steered composite laminates, which is addressed here, had not been reported in the literature before.

Among the methodologies available for damping characterization, the Specific Damping Capacity is considered an adequate approach to study the effect of fiber steering on the modal damping of composite laminates. Therefore, this method is adopted herein. Based on the hypotheses of Kirchhoff plate theory, a dynamic model is formulated by associating the Classical Lamination Theory with the Rayleigh–Ritz (Assumed-Modes) approach. The modeling approach duly accounts for the curvilinear trajectory of the fibers on each lamina. The modal damping factors are calculated using the Strain Energy Method, which is based on the ratio between the stored and the dissipated energies, giving the specific damping capacity (SDC), which can be related to the modal damping factor of each vibration mode. In this paper, the values of natural frequencies and modal damping factors are evaluated for different fiber trajectories in order to verify,

both qualitatively and quantitatively, the influence of fiber steering on natural frequencies and modal damping factors of composite plates. Therefore, the objectives of this paper are: (1) to compare theoretical and experimental dynamic characteristics of constant-stiffness and tow-steered composite plates in terms natural frequencies, modal damping factors, mode shapes and Frequency Response Functions; (2) to correlate the influence of fiber steering fibers with the physical dissipation mechanisms responsible for damping.

FORMULATION

In this work, the procedure for the modeling of damping follows the approach proposed by Adams and Bacon (1973), which is based on the assumption that the dissipated energy is associated to principal stress components at the ply level. For a given displacement field, the specific damping capacity is defined as the ratio of the dissipated strain energy (ΔU) per cycle of vibration to the maximum strain energy (U), i.e.,:

$$\Psi = \frac{\Delta U}{U}. \tag{1}$$

When U and ΔU are computed for the displacement fields corresponding to a set of natural vibration modes, the SDC provides the modal damping factors associated to those modes. Hence, U and ΔU are formulated herein for the tow-steered laminate based on the developments presented by Maheri and Adams (2003).

According the Rayleigh-Ritz method, the transverse displacement field of the plate $w(x,y,t)$ is approximated as:

$$w(x,y,t) = \sum_{m=0}^{\mathrm{M}} \sum_{n=0}^{\mathrm{N}} X_m(x) Y_n(y) q_{mn}(t). \tag{2}$$

The functions $X_m(x)$ and $Y_n(y)$ must be differentiable at least to the maximum order of the derivatives that appear in the expressions of strain energy, and must obey at least the geometric boundary conditions of the problem. Here, these functions $X_m(x)$ and $Y_n(y)$ have been chosen as Legendre polynomials, so that Eq. 2 is rewritten in terms of dimensionless coordinates ($\zeta = 2x/a$ and $\eta = 2y/b$) as follows (Wu *et al.*, 2012):

$$w(\zeta,\eta,t) = (1-\zeta^2)^c (1-\eta^2)^c \sum_{m=0}^{\mathrm{M}} \sum_{n=0}^{\mathrm{N}} X_m(\zeta) Y_n(\eta) q_{mn}(t), \tag{3}$$

where

$$\begin{aligned} X_m(\zeta) &= \frac{1}{2^m} \sum_{k=0}^{m} \binom{m}{k}^2 (\zeta-1)^{m-k} (\zeta+1)^k, \\ Y_n(\eta) &= \frac{1}{2^n} \sum_{k=0}^{n} \binom{n}{k}^2 (\eta-1)^{n-k} (\eta+1)^k. \end{aligned} \tag{4}$$

It should be noticed that the parameter c enables to account for different boundary conditions, c=0,1,2 corresponding to free, simply-supported and clamped edges, respectively. Equation 3 can be written in a compact form as:

$$w(\zeta,\eta,t) = \Phi(\zeta,\eta)\mathbf{q}(t), \tag{5}$$

Then, considering the absence of external forces and applying Lagrange's equations, the equations of motion are found in the form:

$$\mathbf{M}\ddot{\mathbf{q}}(t) + \mathbf{K}\mathbf{q}(t) = \mathbf{0}, \tag{6}$$

with the following associated eigenvalue problem:

$$\left(\mathbf{K} - \omega^2 \mathbf{M}\right)\mathbf{q} = 0, \tag{7}$$

where

$$\mathbf{M} = h\rho \frac{ab}{4} \int_{-1}^{1} \int_{-1}^{1} \Phi^{\mathrm{T}} \Phi d\zeta d\eta, \tag{8}$$

and

$$\mathbf{K} = \frac{ab}{4}\int_{-1}^{1}\int_{-1}^{1}\left\{D_{11}\frac{\partial^2\Phi}{\partial x^2}^{\mathrm{T}}\frac{\partial^2\Phi}{\partial x^2} + 2D_{12}\frac{\partial^2\Phi}{\partial x^2}^{\mathrm{T}}\frac{\partial^2\Phi}{\partial y^2} + D_{22}\frac{\partial^2\Phi}{\partial y^2}^{\mathrm{T}}\frac{\partial^2\Phi}{\partial y^2} \right.$$
$$\left. + 4D_{16}\frac{\partial^2\Phi}{\partial x^2}^{\mathrm{T}}\frac{\partial^2\Phi}{\partial x\partial y} + 4D_{26}\frac{\partial^2\Phi}{\partial y^2}^{\mathrm{T}}\frac{\partial^2\Phi}{\partial x\partial y} + 4D_{66}\frac{\partial^2\Phi}{\partial x\partial y}^{\mathrm{T}}\frac{\partial^2\Phi}{\partial x\partial y}\right\} d\zeta d\eta, \quad (9)$$

where,

$$\mathbf{D} = \sum_{k=1}^{N}\left(\int_{z_{k-1}}^{z_k}\bar{\mathbf{Q}}_k z^2 dz\right) = \sum_{k=1}^{N}\int_{z_{k-1}}^{z_k}\begin{bmatrix}\bar{Q}_{11} & \bar{Q}_{12} & \bar{Q}_{16}\\ \bar{Q}_{12} & \bar{Q}_{22} & \bar{Q}_{26}\\ \bar{Q}_{16} & \bar{Q}_{26} & \bar{Q}_{66}\end{bmatrix}_k z^2 dz = \frac{1}{3}\sum_{k=1}^{N}(z_k^3 - z_{k-1}^3)\bar{\mathbf{Q}}_k, \quad (10)$$

with z_{k-1} and z_k being the lower and upper transverse coordinates of each layer (k) and $\bar{\mathbf{Q}}_k = \mathbf{T}_k^{\mathrm{T}}\mathbf{Q}_k\mathbf{T}_k$.

The stiffness matrix $\mathbf{Q}_k$ is given by:

$$\mathbf{Q}_k = \begin{bmatrix}Q_{11} & Q_{12} & 0\\ Q_{12} & Q_{22} & 0\\ 0 & 0 & Q_{66}\end{bmatrix} \quad (11)$$

where,

$$Q_{11} = \frac{E_1}{1-\nu_{12}\nu_{21}}, \quad Q_{22} = \frac{E_2}{1-\nu_{12}\nu_{21}}, \quad Q_{12} = Q_{21} = \frac{\nu_{12}E_2}{1-\nu_{12}\nu_{21}}, \quad Q_{66} = G_{12}, \quad (12)$$

and $\mathbf{T}_k$ is the transformation matrix of the strain vector from the global coordinate system $(x-y)$ to the principal coordinates $(1-2)$, which is given by

$$\mathbf{T}_k = \begin{bmatrix}c^2 & s^2 & cs\\ s^2 & c^2 & -cs\\ -2cs & 2cs & c^2-s^2\end{bmatrix}^{(k)}, \quad (13)$$

where $c = \cos\theta^{(k)}$ and $s = \sin\theta^{(k)}$. For the tow-steered composite laminates, $\theta^{(k)}$ is function of $x-y$, therefore $\mathbf{T}_k(\theta^{(k)}(x,y))$.

Finally, the strain and kinetic energies are expressed as:

$$U = \frac{1}{2}\mathbf{q}^{\mathrm{T}}\mathbf{K}\mathbf{q}, \quad T = \frac{1}{2}\dot{\mathbf{q}}^{\mathrm{T}}\mathbf{M}\dot{\mathbf{q}}. \quad (14)$$

In addition,

$$\Delta U = \frac{1}{2}\mathbf{q}^{\mathrm{T}}\mathbf{K}_{\mathbf{d}}\mathbf{q}, \quad (15)$$

where

$$\mathbf{K_d} = \frac{ab}{4}\int_{-1}^{1}\int_{-1}^{1}\left\{d_{11}\frac{\partial^2\Phi}{\partial x^2}^{\mathrm{T}}\frac{\partial^2\Phi}{\partial x^2} + (d_{12}+d_{21})\frac{\partial^2\Phi}{\partial x^2}^{\mathrm{T}}\frac{\partial^2\Phi}{\partial y^2} + d_{22}\frac{\partial^2\Phi}{\partial y^2}^{\mathrm{T}}\frac{\partial^2\Phi}{\partial y^2}\right.$$
$$\left. + 2(d_{16}+d_{61})\frac{\partial^2\Phi}{\partial x^2}^{\mathrm{T}}\frac{\partial^2\Phi}{\partial x\partial y} + 2(d_{26}+d_{62})\frac{\partial^2\Phi}{\partial y^2}^{\mathrm{T}}\frac{\partial^2\Phi}{\partial x\partial y} + 4d_{66}\frac{\partial^2\Phi}{\partial x\partial y}^{\mathrm{T}}\frac{\partial^2\Phi}{\partial x\partial y}\right\} d\zeta d\eta, \quad (16)$$

where,

$$\mathbf{d} = \sum_{k=1}^{N}\left(\int_{z_{k-1}}^{z_k}\mathbf{R}_k z^2 dz\right) = \sum_{k=1}^{N}\int_{z_{k-1}}^{z_k}\begin{bmatrix}R_{11} & R_{12} & R_{16}\\ R_{21} & R_{22} & R_{26}\\ R_{61} & R_{62} & R_{66}\end{bmatrix}_k z^2 dz = \frac{1}{3}\sum_{k=1}^{N}(z_k^3 - z_{k-1}^3)\mathbf{R}_k \quad (17)$$

in which $\mathbf{R}_k$ is called "damped stiffness matrix" and is given by $\mathbf{R}_k = \mathbf{T}_k^{\mathrm{T}}\psi_k\mathbf{Q}_k\mathbf{T}_k$. Matrix ψ_k represents the damping properties of the material (Maheri and Adams, 2003), and is given by:

$$\psi_k = \begin{bmatrix}\psi_L & 0 & 0\\ 0 & \psi_T & 0\\ 0 & 0 & \psi_{LT}\end{bmatrix}. \quad (18)$$

The components ψ_L, ψ_T and ψ_{LT} are the longitudinal, transverse and shear specif damping capacities of a unidirectional lamina, respectively.

According to Zabaras and Pervez (1990), the relation between the specific damping capacity and the modal damping factor of the laminate for the $r-$th mode is given by

$$\zeta_r = \frac{1}{4\pi}\frac{\Delta U_r}{U_r} = \frac{1}{4\pi}\frac{\mathbf{q_r}^{\mathrm{T}}\mathbf{K_d}\mathbf{q_r}}{\mathbf{q_r}^{\mathrm{T}}\mathbf{K}\mathbf{q_r}} \tag{19}$$

Tow-steered composite plates

Many strategies can be adopted to define the fiber trajectories in tow-steered laminates. In this paper, accounting for typical limitations of AFP machines, which precludes the use of complicated paths, especially those exhibiting small radii of curvature, the fiber course is chosen so as to vary only along one of the coordinates. These are called constant curvature paths (Falcó *et al.*, 2014b). Figure 1 shows the fiber paths on and individual ply, as well as the two angles T_0 and T_1, which are used to parameterize the curve indicated with thick line, according to (Blom *et al.*, 2009):

$$\theta(x) = \phi + asin\left(sinT_0 + (sinT_1 - sinT_0) * \left(\frac{x}{a} + \frac{1}{2}\right)\right), \tag{20}$$

where T_0 and T_1 are fiber orientations at the left and right edges of the plate, respectively, the dimensions of which are a and b in directions x and y, respectively. The paths of the other fibers are obtained by shifting the one defined by Eq. 20 along the y-axis. Following Gurdal and Olmedo (1993), the tow-steered laminate is identified by the notation $< T_0, T_1 >$. In Eq.20, ϕ represents the orientation of an individual ply with respect to the laminate reference frame, just as is the case for traditional, non-steered composites. For example, a non-steered composite laminate presenting a lay-up with two layers [0, 90] has ϕ equal to 0° for the first one and equal to 90° for the second; for the tow-steered counterpart, the notation is $[< T_0, T_1 >, 90 + < T_0, T_1 >]$.

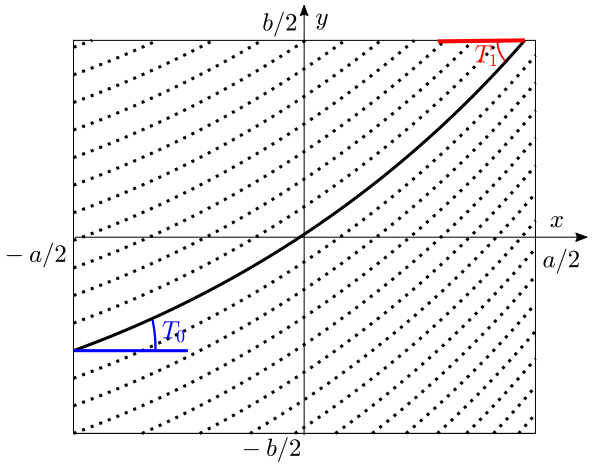

Figure 1: Constant curvature fiber trajectories in a tow-steered ply.

ANALYSES AND RESULTS

Figure 2(a) shows the automated fiber placement machine, settled at Lightweight Structures Laboratory (LEL) of the Institute for Technological Research (IPT), executing the process of tow steering technique in the manufacture of a rectangular laminate. Figure 2(b) presents the dynamic test rig which belongs to Laboratory of Dynamics and Adaptive Structures from Aeronautics Institute of Technology (ITA). The modal analysis to obtain natural frequencies, vibration modes and modal damping factors were done using the Siemens LMS-SCADAS Mobile measurement equipment with eight channels. Velocity measurement was made using a Polytec CLV-2534 laser vibrometer, the acceleration was measured with mini-accelerometers PCB brand Piezotronics model 352C22, and the excitation force was applied with an electromagnetic mini shaker from TMS (The Modal Shop) with an aluminum stinger and 208C03 PCB load cell. Finally, the signal processing was made using the software LMS Test.Lab 17 from Siemens and the Structures Acquisition-Spectral Testing package.

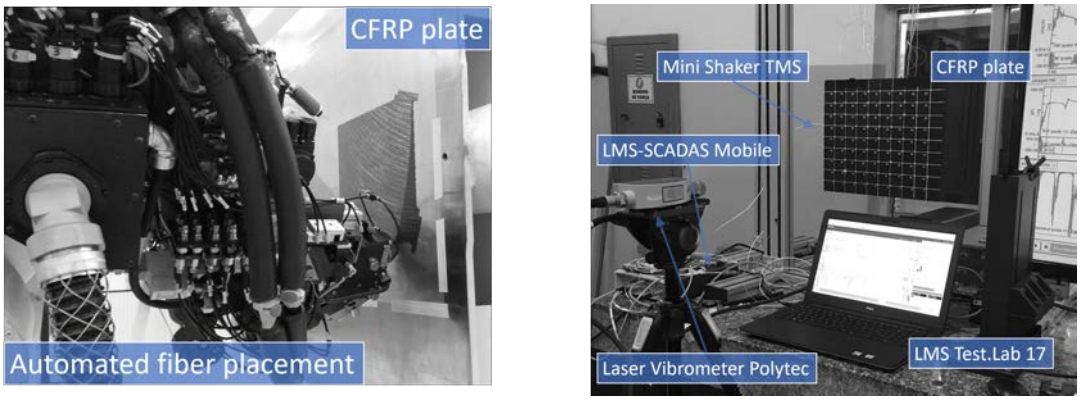

(a) Automated fiber placement.

(b) Test rig for vibration measurements

Figure 2: Experimental apparatus for manufacture composite plates and dynamic analyses.

Following Blom *et al.* (2009), the minimum turning radius for tow-steered composite plates which can be manufactured with AFP resulting in a laminate with acceptable manufacturing quality, calculated according to equation 21, is 625 mm. Therefore, in this work the values of T_0 and T_1 (see equation 20) were chosen to be $-20°$ and $-50°$, respectively. This results in a turning radius of 790 mm.

$$r = \frac{a}{(sinT_1 - sinT_0)}. \tag{21}$$

The two laminates subjected to dynamic tests were defined with six layers. The first plate is a constant stiffness composite and presents a lay-up [0, 90, 90]$_s$ as shown in Figure 3 (a). The second plate (Fig.3(b)) is a tow-steered plate with lay-up $< T_0, T_1 >$ with lay-up $[< -50, -20 >, < 40, 70 >, < 40, 70 >]_s$.

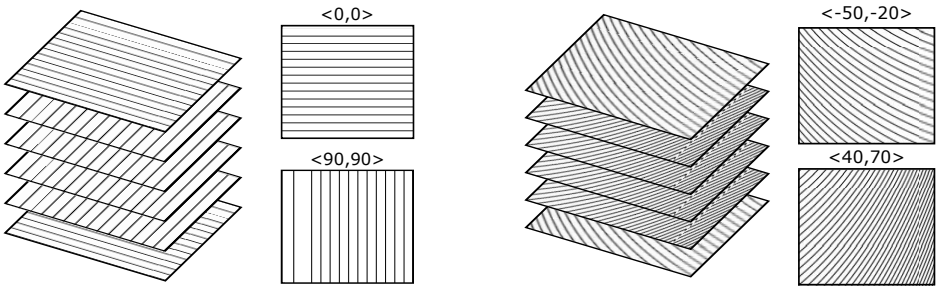

(a) (b)

Figure 3: Two plates under study: (a) constant-stiffness composite plate with lay-up $[0, 90, 90]_s$ and (b) tow-steered composite plate with lay-up $[< -50, -20 >, < 40, 70 >< 40, 70 >]_s$.

The material properties of carbon fiber and epoxy resin from Hexcel with a trade mark name as Hexply®, and geometric parameters of the laminates under study of dimensions $a \times b \times h$ (length $\times$ width $\times$ total laminate thickness, respectively) are presented in Table 1.

Table 1: Material properties of CFRP Hexply ® and the plates dimensions.

E_1 (GPa)	E_2 (GPa)	G_{12} (GPa)	ν_{12}	ψ_L (%)	ψ_T (%)	ψ_{LT} (%)	ρ (kg/m^3)	a (mm)	b (mm)	h (mm)
127.85	8.30	4.62	0.30	3.36	8.04	13.20	1632	335	285	1.104

These properties were determined from experimental FRFs encompassing the first six vibration modes of the non-steered and tow-steered plates. The problem of identifying material properties from FRFs is an "inverse problem", which was formulated as an optimization problem solved by using Genetic Algorithms.

The plates with constant and variable stiffness were analyzed under free boundary conditions. They were suspended vertically with nylon threads; the excitation was introduced as white noise with the frequency range [0-512 Hz] through and aluminum stinger connecting a load cell to the shaker, in such a way that the excitation load is applied perpendicularly to the plate. The plates were discretized in a 81-point mesh, where the acceleration signals were obtained with a miniature piezoelectric accelerometer and the velocity signals with a laser vibrometer.

Table 2 shows the numerical (R-R) and experimental results for natural frequencies and modal damping factors. The differences for the natural frequencies are below 2%, showing good correlation between the model and experimental results. However, the modal damping values shown in Table 2 present a weak correlation between the experiment and numerical results, especially for the first mode of vibration. Search for improvement of this correlation is under development.

Table 2: Comparison of the numerical results from the Rayleigh-Ritz model and experimental results obtained for the **constant-stiffness** composite plate and **free-free** (FFFF) boundary condition.

		Mode 1	Mode 2	Mode 3	Mode 4	Mode 5	Mode 6
Freq. (Hz)	R-R	21.05	72.25	76.54	84.01	87.28	136.44
	Exp.	**21.21**	**73.59**	**76.48**	**85.03**	**88.98**	**134.33**
	Diff.(%)	-0.75	-1.82	0.08	-1.20	-1.90	1.57
SDC (%)	R-R	12.92	3.93	3.54	6.23	5.68	7.33
	Exp.	**46.51**	**3.68**	**3.57**	**8.86**	**6.05**	**6.25**
	Diff.	-72.21	6.77	-0.82	-29.69	-6.04	17.23

Figure 4 shows de mode shapes corresponding to the first three natural frequencies for the constant-stiffness plate. One can see the excellent correlation between the numerical and experimental modal displacement fields. The first mode (21.05 Hz) presents a twisting-type deformation pattern while the second mode (72.25 Hz) and third mode (76.54 Hz) are pure bending-type deformation about the x-axis and y-axis respectively.

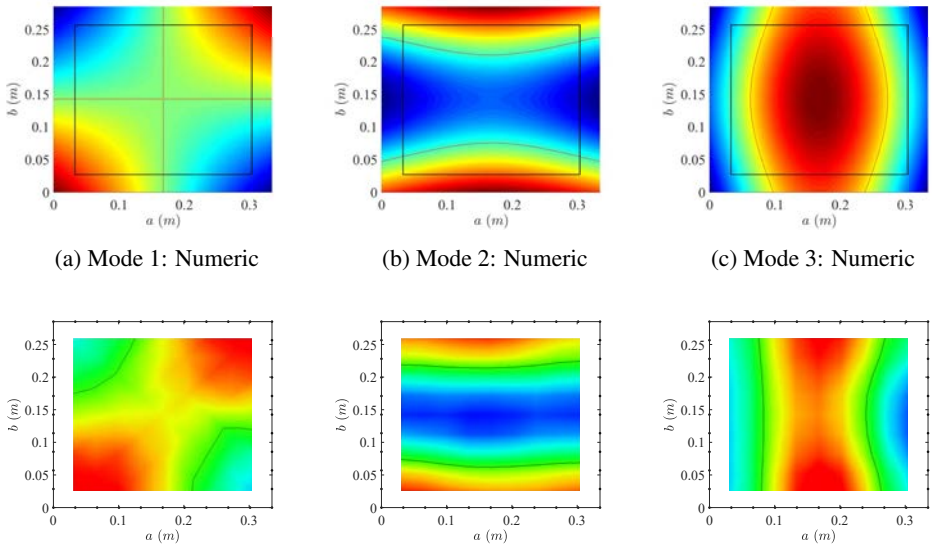

(a) Mode 1: Numeric (b) Mode 2: Numeric (c) Mode 3: Numeric

(d) Mode 1: Experimental (e) Mode 2: Experimental (f) Mode 3: Experimental

Figure 4: Comparison between the experimental and numerical results for the first three modal shapes of the constant-stiffness plate.

From Table 2 the numerical SDC predictions are 12.92%, 3.93% and 3.54% for the first, second and third mode of vibration, respectively. Inspecting Table 1, one can see that there are three parameters that contribute to the damping ψ_L, ψ_T and ψ_{LT}. Those contributions are associated to the stresses components in the fiber direction (ψ_L), in the direction perpendicular to the fibers (ψ_T), and to the in-plane shear stress (ψ_{LT}), which are nearly exclusively determined by the matrix (Tang and Yan, 2018), having hence relatively high SDC's. It is relevant to highlight that the modal damping will be a weighted average between the longitudinal, transverse and shearing effects of the material damping. However, the main reason behind the higher damping capacity of the FRP composites, compared to metals, is the viscoelasticity of the polymeric matrix (Treviso *et al.*, 2015; Chandra *et al.*, 1999), which makes the first mode to present a high damping

coefficient due to the dominant twisting-deformation type, exciting the shearing of the viscoelasticity of the matrix. The second and third modes are a pure bending-deformation type, which induces more the deflection of the fibers in detriment of the matrix, therefore, showing less damping.

Figure 5(a) presents the constant-stiffness composite plate with 81 measured points. The frequency response functions were obtained by applying the excitation force at position 31 and measuring the acceleration at 81 different points of the measurement grid. Figure 5(b) shows the nodal lines of the first six modes (blue lines), which present a well-defined pattern. Figure 5(b) also indicates the shaker excitation position (location 4) and the accelerometer positions (locations 4 and 31) to obtain the FRF presented in Figure 6, which shows the comparison between numerical and experimental FRFs for measurements at points 4 and 31. One can see that both results present a quite good correlation. The 81 FRFs are used in a modal identification procedure to identify the experimental modal shapes, which are shown in Figure 4.

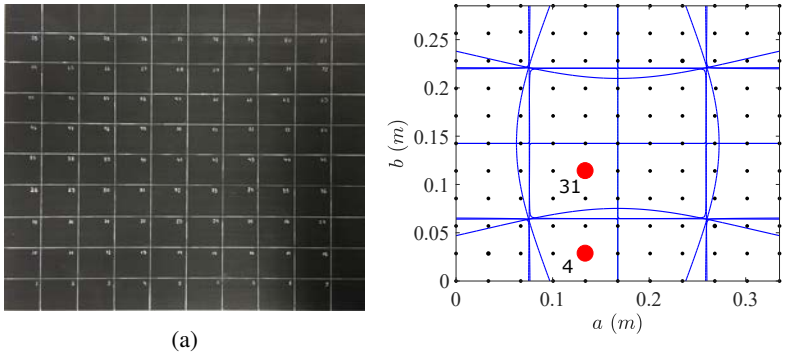

(a) (b)

Figure 5: (a) Constant-stiffness composite plate with 81 measured points, (b) nodal lines of the first six modes (blue), shaker excitation position (location 4) and the accelerometer positions (locations 4 and 31) to obtain the FRF's.

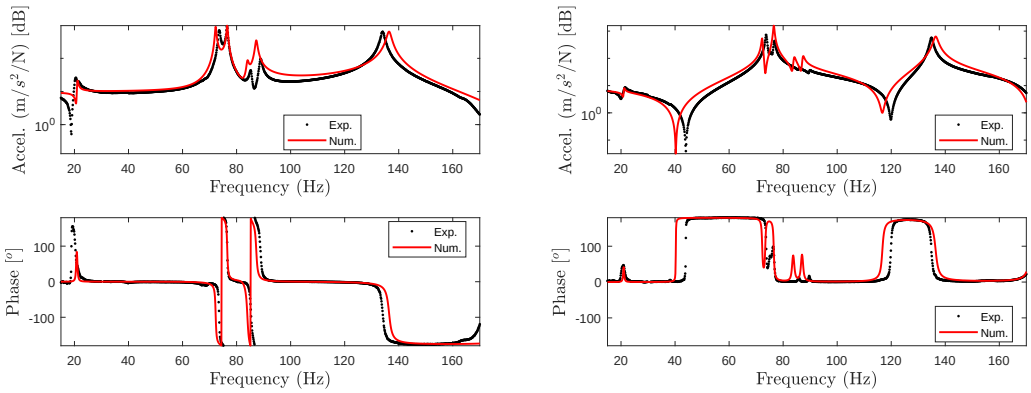

(a) Region 4. (b) Region 31.

Figure 6: Comparison between experimental and numerical results for the FRFs for the constant-stiffness plate.

Table 3 presents the numerical and experimental results for natural frequencies and modal damping factors of the tow-steered composites plates. The maximum difference for the natural frequencies is 7.98% for the fifth mode of vibration, also showing an excellent correlation between the model and the physics. However, for the specific damping capacity, the difference between numeric and experiment results is much higher.

Although the tests to measure the damping in the tow-steered plate presents the same issues faced for the constant stiffness plate, some additional effects can be responsible for the deviations observed. Figure 7(a) and Figure 7(b) show images obtained from ultrasound non-destructive testing of the constant-stiffness plate and the tow-steered plate, respectively. It can be clearly seen that this later presents many internal defects associated to the fiber deposition, generating regions with gaps. One can presume that high density of gaps in the tow-steered plate can have a strong influence on the dissipation mechanism (Chandra *et al.*, 1999; Tang and Yan, 2018). There are some ways to control the occurrence of gaps in a tow-steered plate (Falcó *et al.*, 2014a), which is under study.

Table 3: Comparison of the numerical results from the Rayleigh-Ritz model and experimental results obtained for the **tow-steered** composite plate and **free-free** (FFFF) boundary condition.

		Modo 1	Modo 2	Modo 3	Modo 4	Modo 5	Modo 6
Freq. (Hz)	R-R	28.73	52.41	71.14	93.01	111.03	158.57
	Exp.	**29.78**	**51.44**	**73.25**	**90.60**	**102.83**	**150.51**
	Diff.(%)	-3.52	1.89	-2.88	2.66	7.98	5.36
SDC (%)	R-R	11.58	4.91	4.58	5.31	5.13	4.72
	Exp.	**35.98**	**28.82**	**8.06**	**7.26**	**10.29**	**12.06**
	Diff.	-67.81	-82.96	-43.15	-26.86	-50.17	-60.89

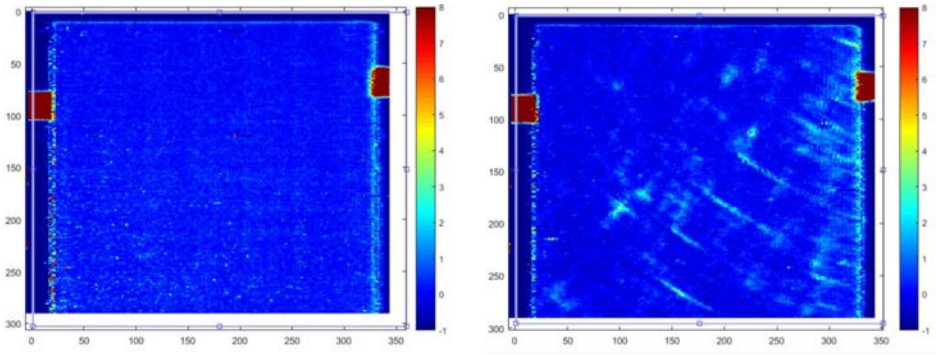

(a) Constant-stiffness (b) Tow-steered

Figure 7: Non-destructive testing using ultrasound image of the constant-stiffness and two-steered plate.

Figure 8 shows the mode shapes corresponding to the first three natural frequencies of the tow-steered plate. One can see the excellent correlation between the numerical and experimental modal deflections. The first mode (28.73 Hz) still presents a twisting-type deformation; however, there is a combination of twisting and the bending deformation. The second (52.41 Hz) and third mode (71.14 Hz), differently from the constant-stiffness plate, is a combination of different types of deformation. Now one can see the strong influence of tow steering fiber on the modal shape of vibration, which undoubtedly controls the damping mechanism in the same way as it influences the natural frequencies.

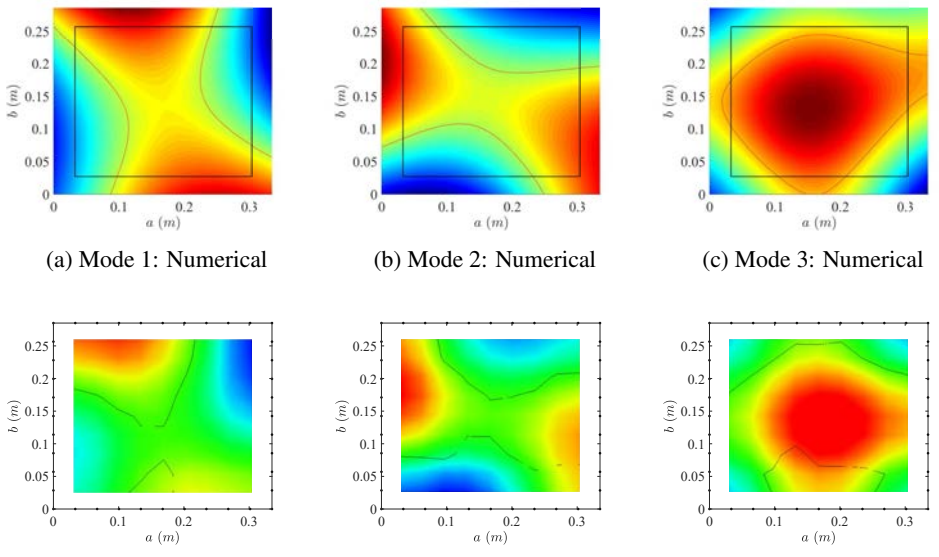

(a) Mode 1: Numerical (b) Mode 2: Numerical (c) Mode 3: Numerical

(d) Mode 1: Experimental (e) Mode 2: Experimental (f) Mode 3: Experimental

Figure 8: Comparison between the experimental and numerical results for the first three modal shapes for **tow-steered** plate.

In Table 3 the numerical SDC's are 11.58%, 4.91% and 4.58% for the first, second and third modes of vibration, respectively. Looking at Table 2, the first mode SDC of the tow-steered plate decreases because of the lower influence of the in-plane shear stress (ψ_{LT}), increasing the influence of normal stresses in the fiber direction (ψ_L) and of the normal stresses in the direction perpendicular to the fibers (ψ_T). An opposite effect happens in the second and third modes when the tow-steering increases the shearing of the matrix, forcing a combination of deflection mechanisms, which is the most critical effect of the tow-steering technique.

Figure 9(a) presents the tow-steered composite plate with 81 measured points. The FRF's were obtained by applying the excitation force at position 1. Figure 9(b) shows the nodal lines of the first six modes (blue lines), which present a complex pattern, which clarifies the deflection mechanism of tow-steered plates in the modal shapes. Figure 10 shows the comparison between numerical and experimental FRFs at points 1 and 74. Once again, one can see that both results present quite good correlation. One can conclude that the tow steering technique is indeed a powerful tool to achieve desired modal characteristics of the plate. It is also clear that a trade-off between the natural frequencies, modal shapes and damping should be analyzed carefully, which requires the use of optimization strategies.

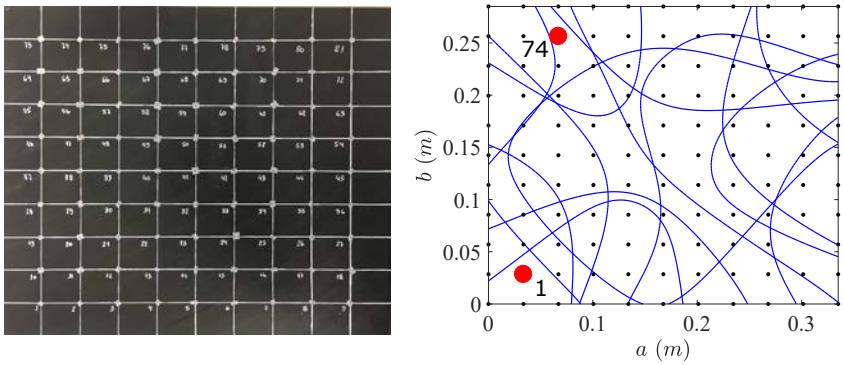

Figure 9: (a) Tow-steered composite plate with 81 measured points, (b) nodal lines of the first six modes (blue), shaker excitation position (location 1) and the accelerometer position (location 1 and 74) to obtain the FRF functions.

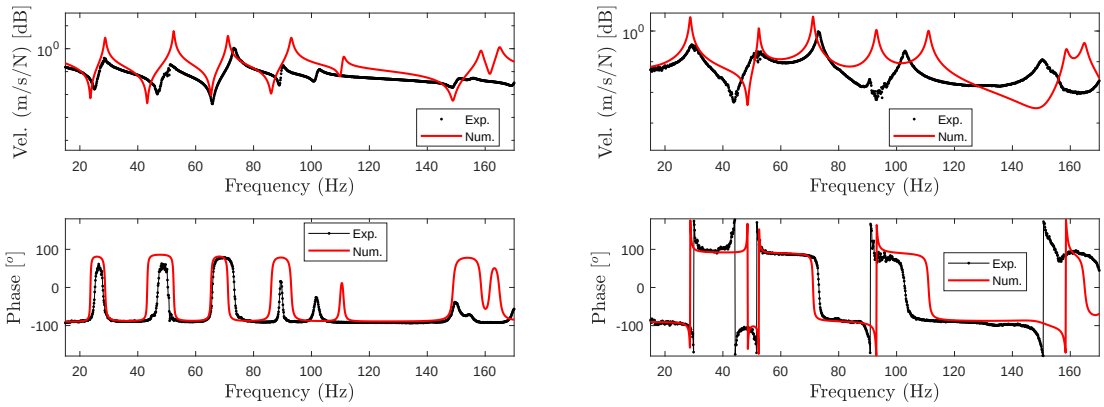

(a) Region 1.

(b) Region 74.

Figure 10: Comparison between experimental and numerical results for the FRFs for the tow-steered plate.

CONCLUSION

This work presented an experimental and numerical assessment of the influence of fiber trajectory on the natural frequencies, specific damping capacities, and natural vibration modes of constant-stiffness and tow-steered composite plates. In the present investigation, the steered configurations considered were defined by only two geometrical parameters, T_0 and T_1. A numerical procedure has been developed to enable the calculation of specific damping capacities of tow steered composites. It has been shown that a semi-analytical Ritz-type modeling combined with the Classical Lamination Theory was capable of providing a sufficiently accurate dynamic model of tow steered plates. Due to the typical low number of degrees-of-freedom, such a model is very convenient to alleviate the computation cost involved in the analyses.

The experimental and numerical values of the natural frequencies and mode shapes correlated quite well ,while the modal damping presents a weak relationship for both plates. This bad correlation can be related to many issues, such as some characteristics of the experimental set-up and the different techniques used to measure the modal damping. Understanding this divergence on the damping measurements and also performing new experiments are currently under development. One also presumes that manufacturing defects, such as gaps identified in the tow-steered plate, can exert influence on the dissipation mechanism. This mechanism is determined by the three material parameters ψ_L, ψ_T and ψ_{LT}, which are associated to each of the three stress components at the level of each ply.

Finally, one can conclude that the fiber curvature induces complex patterns of mode deflection, affecting the frequency and the damping of the plate. It is also clear that a trade-off between the natural frequencies, modal shapes and damping should be analyzed carefully, each of which favors a particular dynamic feature. Hence, in these cases, numerical multi-objective optimization must be used to achieve specific design goals. This work confirms that fiber steering can be an effective strategy for the design of composite laminates regarding their dynamic behavior. In particular, it has been found that damping levels can be increased by exploring fiber steering.

ACKNOWLEDGEMENTS

The authors acknowledge the National Council for Scientific and Technological Development (CNPq) (grants #301633/2013-3, #402238/2013-3 and #145439/2015-1), the National Institute of Science and Technology of Smart Structures in Engineering (INCT − EIE), FAPEMIG, Fundação de Apoio ao Instituto de Pesquisas Tecnológicas (FIPT) and São Paulo State Research Agency (FAPESP) grant #2015/20363-6 for the financial support to their research work.

REFERENCES

Abbaslou, A. and Maheri, M., 2016. "Prediction of the damping properties of fiber-reinforced polymer composite panels with arbitrary geometries". *Proceedings of the Institution of Mechanical Engineers, Part C: Journal of Mechanical Engineering Science*, Vol. 232, No. 2, pp. 275–283.

Adams, R. and Bacon, D., 1973. "Effect of fibre orientation and laminate geometry on the dynamic properties of cfrp". *Journal of Composite Materials*, Vol. 7, No. 4, pp. 402–428.

Akhavan, H. and Ribeiro, P., 2011. "Natural modes of vibration of variable stiffness composite laminates with curvilinear fibers". *Composite Structures*, Vol. 93, No. 11, pp. 3040 – 3047. ISSN 0263-8223.

Berthelot, J.M., 2006. "Damping analysis of laminated beams and plates using the ritz method". *Composite Structures*, Vol. 74, No. 2, pp. 186–201.

Blom, A.W., Lopes, C.S., Kromwijk, P.J., Gurdal, Z. and Camanho, P.P., 2009. "A theoretical model to study the influence of tow-drop areas on the stiffness and strength of variable-stiffness laminates". *Journal of composite materials*, Vol. 43, No. 5, pp. 403–425.

Chandra, R., Singh, S. and Gupta, K., 1999. "Damping studies in fiber-reinforced composites–a review". *Composite structures*, Vol. 46, No. 1, pp. 41–51.

Falcó, O., Lopes, C., Naya, F., Sket, F., Maimí, P. and Mayugo, J., 2017. "Modelling and simulation of tow-drop effects arising from the manufacturing of steered-fibre composites". *Composites Part A: Applied Science and Manufacturing*, Vol. 93, No. Supplement C, pp. 59 – 71.

Falcó, O., Mayugo, J.A., Lopes, C.S., Gascons, N., Turon, A. and Costa, J., 2014a. "Variable-stiffness composite panels: As-manufactured modeling and its influence on the failure behavior". *Composites Part B: Engineering*, Vol. 56, pp. 660–669.

Falcó, O., Mayugo, J., Lopes, C., Gascons, N., Turon, A. and Costa, J., 2014b. "Variable-stiffness composite panels: As-manufactured modeling and its influence on the failure behavior". *Composites Part B: Engineering*, Vol. 56, pp. 660–669.

Guimarães, T.A.M., 2016. *Contribuição ao estudo do comportamento dinâmico e aeroelástico de laminados compósitos de rigidez variável*. Ph.D. thesis, Federal University of Uberlândia - Scholl of Mechanic Engineering.

Gurdal, Z. and Olmedo, R., 1993. "In-plane response of laminates with spatially varying fiber orientations-variable stiffness concept". *AIAA journal*, Vol. 31, No. 4, pp. 751–758.

Hwang, S., Gibson, R. and Singh, J., 1992. "Decomposition of coupling effects on damping of laminated composites under flexural vibration". *Composites Science and Technology*, Vol. 43, No. 2, pp. 159–169.

Maheri, M.R. and Adams, R., 2003. "Modal vibration damping of anisotropic frp laminates using the rayleigh–ritz energy minimization scheme". *Journal of sound and vibration*, Vol. 259, No. 1, pp. 17–29.

Ribeiro, P., Akhavan, H., Teter, A. and Warmiński, J., 2014. "A review on the mechanical behaviour of curvilinear fibre composite laminated panels". *Journal of Composite Materials*, Vol. 48, No. 22, pp. 2761–2777.

Rodrigues, J., Ribeiro, P. and Akhavan, H., 2013. "Experimental and finite element modal analysis of variable stiffness composite laminated plates". In *Proceedings of the 11th Biennial International Conference on Vibration Problems (ICOVP-2013)*. p. 30.

Saravanos, D.A. and Chamis, C.C., 1990. "Unified micromechanics of damping for unidirectional and off-axis fiber composites". *Journal of Composites, Technology and Research*, Vol. 12, No. 1, pp. 31–40.

Tang, X. and Yan, X., 2018. "A review on the damping properties of fiber reinforced polymer composites". *Journal of Industrial Textiles*, p. 1528083718795914.

Treviso, A., Van Genechten, B., Mundo, D. and Tournour, M., 2015. "Damping in composite materials: Properties and models". *Composites Part B: Engineering*, Vol. 78, pp. 144–152.

Wu, Z., Weaver, P.M., Raju, G. and Chul Kim, B., 2012. "Buckling analysis and optimisation of variable angle tow composite plates". *Thin-Walled Structures*, Vol. 60, pp. 163–172.

Zabaras, N. and Pervez, T., 1990. "Viscous damping approximation of laminated anisotropic composite plates using the finite element method". *Computer methods in applied mechanics and engineering*, Vol. 81, No. 3, pp. 291–316.

RESPONSIBILITY NOTICE

The author(s) is (are) the only responsible for the printed material included in this paper.